

Calibration of a Second-Order Traffic Flow Model Using a Metamodel-assisted Differential Evolution Algorithm

Kallirroi N. Porfyri¹, Ioannis K. Nikolos¹, Anargiros I. Delis¹, Markos Papageorgiou¹

Abstract—With the increasingly widespread use of traffic flow simulation models, several questions concerning the reliability, efficiency and accuracy of such models need to be addressed convincingly. In general, the most time-efficient traffic flow models are based on the macroscopic approach to describe traffic dynamics. Macroscopic models reproduce the evolution of aggregated traffic characteristics over time and space with respect to observable variables, such as flow and speed, requiring much less computational time, compared to microscopic ones. This work assesses a second-order macroscopic gas-kinetic traffic flow (GKT) model and its numerical implementation using real traffic data from a motorway network in the U.K., where recurrent congestion originated from high on-ramp flows during the morning peak hours is observed. A parallel, metamodel-assisted Differential Evolution (DE) algorithm is employed for the calibration of the model parameters, and numerical simulations demonstrate that the DE algorithm can be a very promising method for the calibration of such traffic flow models.

I. INTRODUCTION

During the last decades, traffic flow simulation models have attracted a rapidly growing interest due to the need for improvements on safety, quality, efficiency and reliability of transportation systems, as well as the need to assess and optimize the highway traffic flow. However, several questions have been raised about the accuracy and applicability of such models when compared against actual measured traffic flow data. Hence, to ensure the validity of those models in performing real-world simulations and provide results that are credible and promising, the application of calibration and validation processes is mandatory.

In general, traffic simulation models are classified, according to the level of detail they use, as microscopic or macroscopic. Specifically, microscopic simulation models describe traffic flow behavior at a high level of detail by capturing the behavior of each individual vehicle, while macroscopic approaches represent traffic in lesser detail by using aggregated variables, such as flow, density and mean speed [1]. In fact, the feature of macroscopic models to call for a relatively small number of partly directly measurable parameters, compared to microscopic ones, results in a less demanding and computationally expensive calibration and validation process and, therefore, in a more versatile development of such models for real applications.

The macroscopic traffic flow models, depending on the number of differential equations they involve, can be categorized as first-, second- or higher-order models. The approaches of the class of first-order models, originally developed by Lighthill–Whitham–Richards (LWR model) [2], consist of the continuity equation, which governs the evolution of traffic density, and a static flow-density relationship (fundamental diagram). However, these models suffer from several limitations and they prove less adequate to describe complicated dynamics of traffic flow; in particular, they do not allow for variations of speed around the equilibrium fundamental diagram and they fail to replicate some phenomena observed in real traffic, such as the hysteresis and capacity drop, the stop-and-go waves at bottlenecks, as well as the diffusion of traffic platoons. The second- or higher-order models, with the pioneer among them PW (Payne Whitham) model [3], utilize an additional dynamic equation, the momentum one, to describe flow/speed dynamics. Although such models have the potential to reproduce the above-mentioned complicated phenomena with higher accuracy when contrasted to real traffic data, they include a higher number of parameters, and small changes to them may result in very different prediction outcomes; consequently, they call for a complex but compulsory calibration process to enhance their prediction accuracy.

As pointed out in [4], the validation process is the ultimate criterion for assessing the accuracy of representing real traffic phenomena, and hence the usefulness of an existing or new macroscopic traffic flow model. However, relatively few works, which also include methods for solving the parameter estimation problem, are available for the calibration and validation process of macroscopic models. Examples are the deterministic complex algorithm of Box in [5]–[10], the deterministic Nelder-Mead algorithm employed in [11], [12], the stochastic genetic algorithm in [13] and the stochastic cross-entropy method utilized in [13], [14]. The goal of the current study is to test the second-order GKT model [15]–[18] with respect to its accuracy in the reproduction of the congestion created at freeways close to on/off-ramps, using real traffic data from a freeway stretch in UK. A recently developed relaxation finite-volume scheme is utilized for the numerical approximation, in space and time, of the underlying partial differential equations [15]. The optimization algorithm considered here is a recently developed parallel, surrogate-model-assisted, Differential Evolution algorithm [19], [20].

¹School of Production Engineering & Management, Technical University of Crete, Chania 73100, Greece. kporfyri@isc.tuc.gr, jnikolo@dpem.tuc.gr, adelis@science.tuc.gr, markos@dssl.tuc.gr.

II. THE GKT MODEL

Here, we briefly recall basic definitions and equations concerning the second-order GKT model [15]–[18]. Let $\rho(x, t)$ denote the traffic density (number of vehicles per unit length) as a function in space, x , and time, t ; $u(x, t)$ the average speed of vehicles; while the traffic flow rate (number of vehicles per unit of time) is given as $q(\rho, u) = \rho(x, t)u(x, t)$. The GKT model in conservation law form with sources reads as

$$\partial_t \rho + \partial_x(\rho u) = r_{rmp}, \quad (1)$$

$$\partial_t(\rho u) + \partial_x(\rho u^2 + \theta \rho) = \rho \left(\frac{V_e^*(\rho) - u}{\tau} \right) + h_{rmp} \quad (2)$$

where the source terms r_{rmp} and h_{rmp} on the right-hand sides of (1) and (2) reflect the impact of traffic flow from on-ramps (or to off-ramps) on the main road. According to [18], the term r_{rmp} denotes the effective source density that is only active within the merging (diverging) sections with length l_{rmp} and inflow $q_{rmp} > 0$ from (or outflow $q_{rmp} < 0$ to) the ramps, determined as

$$r_{rmp}(x, t) = \begin{cases} \frac{q_{rmp}(t)}{l_{rmp}} & \text{if } x \text{ inside merging zone,} \\ 0 & \text{elsewhere.} \end{cases} \quad (3)$$

The source term h_{rmp} in (2) describes changes of the macroscopic local speed by assuming that on-ramp vehicles merge to the main road at speed $u_{rmp} < u$. On the contrary, the drivers considered to leave the main road reduce their speed to u_{rmp} before they diverge to the off-ramp. Hence, this term can be expressed as

$$h_{rmp}(x, t) = \frac{q \cdot r_{rmp}}{\rho} + \frac{(u_{rmp} - u)|q_{rmp}|}{l_{rmp}}. \quad (4)$$

Further, the pressure-like term θ in (2) is a density-dependent fraction $A(\rho)$ of the squared velocity $\theta = A(\rho)u^2$, where $A(\rho)$ is given by the Fermi function as

$$A(\rho) = A_0 + \delta A \left[1 + \tanh \left(\frac{\rho - \rho_{cr}}{\delta \rho} \right) \right], \quad (5)$$

where ρ_{cr} is the critical density, reflecting the boundary for the transition from the free flow to congested traffic state, A_0 and $A_0 + 2\delta A$ represent the variance pre-factors between the aforementioned two states, while $\delta \rho$ is the width of the transition region. Typical range of values for the constant parameters A_0 , δA , and $\delta \rho$, along with other typical used model parameters for the GKT model can be found in [15]–[18]. Moreover, the model includes a traffic relaxation term that maintains the concentration of velocity in equilibrium state, with $V_e^*(\rho) = (\rho, u, \rho_\alpha, u_\alpha)$ being the dynamic equilibrium speed, depending not only on the local (ρ, u) but also on the non-local traffic state (ρ_α, u_α) . Thus, the dynamic equilibrium speed, toward which the average speed relaxes, is determined as

$$V_e^*(\rho) = u_{max} \left[1 - \frac{\theta + \theta_\alpha}{2A\rho_{max}} \left(\frac{\rho_\alpha T}{1 - \rho_\alpha/\rho_{max}} \right)^2 B(\delta u) \right]. \quad (6)$$

According to (6), the dynamic equilibrium speed is computed as the maximum desired speed, denoted as u_{max} , minus a braking non-local term in response to necessary deceleration maneuvers in traffic flow at the downstream interaction location $x_\alpha = x + \gamma(1/\rho_{max} + T \cdot u)$, where T is the desired time gap, ρ_{max} is the maximum density, and γ is a scale parameter. Finally, $B(\delta u)$ is a Boltzmann (interaction) factor that contains the standard normal distribution and the Gaussian error function, given as

$$B(\delta u) = 2 \left[\delta u \frac{e^{-\delta u^2/2}}{\sqrt{2\pi}} + (1 + \delta u^2) \int_{-\infty}^{\delta u} \frac{e^{-y^2/2}}{\sqrt{2\pi}} dy \right]. \quad (7)$$

The above monotonically increasing term describes the dependence of the braking interaction on the dimensionless velocity difference $\delta u = (u - u_\alpha)/\sqrt{\theta + \theta_\alpha}$, taking into account the velocity and variance at the actual position x and the interaction point x_α , respectively. The major difference comparing to other macroscopic traffic flow models is the non-local character of the GKT model. Specifically, this nonlocality has smoothing attributes like those of a diffusion or viscosity term, but its effect is more realistic as it is forwardly directed, which means that vehicles react on density or velocity gradients in front of them. Moreover, unlike other macroscopic models, the steady-state (equilibrium) speed-density relation of GKT model, $V_e^*(\rho)$, is implicitly given from the steady-state condition of homogeneous traffic. To numerically approximate system (1)-(2), we apply a higher-order finite-volume relaxation scheme. The spatial discretization is based on a fifth-order Weighted Essential Non-Oscillatory-type (WENO) interpolant approach, while for the temporal discretization a third-order implicit-explicit (IMEX) Runge-Kutta method was considered. The superiority and performance of this higher-order scheme, compared to low-order ones, in traffic flow simulations has been recently demonstrated in [15], where a detailed description of the spatial and temporal discretization schemes can be found.

III. MODEL CALIBRATION

The model parameter calibration constitutes an integral part of the development and application of any macroscopic traffic flow model. In fact, the reliability and versatility of the model to reflect different traffic conditions of a freeway network with the highest possible level of accuracy is of major importance. However, the assignment of appropriate values to the unknown model parameters is a challenging problem, because of the highly non-linear nature of the model equations.

In this study, we present a methodology for the calibration of the GKT model parameter vector $\mathbf{X} = [u_{max}, \rho_{max}, \rho_{cr}, T, \gamma, \tau, A_0, \delta A, \delta \rho]$ so as to minimize the discrepancy between the model estimations and real measured traffic data, using an appropriate cost function, hereafter denoted by $f(\mathbf{X})$. The calibration of the GKT model is defined as a problem of finding an optimal parameter vector \mathbf{X} subject to (1) and (2) for all $\mathbf{X} \in \Omega$, where Ω is a constrained admissible region of the parameter space,

determined by physical considerations. Such a calibration process takes the form of a multi-extrema continuous optimization problem, see e.g. [14], in which the cost function exhibits multiple local minima, which gradient-based solution algorithms typically fail to avoid. In this work, we apply for the first time in the context of traffic flow modelling a recently developed parallel, metamodel-assisted Differential Evolution algorithm for the aforementioned calibration problem, that is able to handle such complex problems with multiple local minima [19], [20].

A. Metamodel-assisted Differential Evolution (DE) algorithm

During the last decades, Evolutionary Algorithms (EAs) have been extensively used in many different optimization problems, as a versatile and robust tool able to deal with demanding high-dimensional real-world problems; however, such problems ask for significantly increased computational resources. In order to overcome this barrier, the use of surrogate models (metamodels), in conjunction with parallel processing, appears to be mandatory. DE has proven to be very robust and computationally efficient, compared to other types of EAs, see for example the references in [19], [20].

Given a cost function $f(\mathbf{X}): \mathbb{R}^n \rightarrow \mathbb{R}$, the objective is the minimization of its value by optimizing the values of the parameter set $\mathbf{X} = (x_1, x_2, \dots, x_n)$, $x_i \in \mathbb{R}$. During the optimization process, the value of each parameter x_i is bounded between pre-specified upper and lower values, $x_i^{(L)} \leq x_i \leq x_i^{(U)}$, $i = 1, \dots, n$. Starting the algorithm, the N_p individuals (chromosomes) of the initial population of candidate solutions are randomly initialized within the given boundaries as:

$$x_{k,i}^{(0)} = r \cdot (x_i^{(U)} - x_i^{(L)}) + x_i^{(L)}, \quad k = 1, \dots, N_p, i = 1, \dots, n, \quad (8)$$

where r denotes a random generated number with uniform probability distribution within the range $[0, 1]$. The alteration of the population is mainly based on differential mutation, where a triplet of randomly selected different individuals is used to generate a new chromosome by adding a weighted difference among the two individuals of the triad to the third one (donor). Subsequently, the perturbed individual and the current population member (parent) are subjected to a crossover recombination, generating in this way the final candidate solution

$$x_{k,i}^{(G+1)} = \begin{cases} x_{C_{k,i}}^{(G)} + F \cdot (x_{A_{k,i}}^{(G)} - x_{B_{k,i}}^{(G)}) & \text{if } (r \leq C_r \vee i = i^*) \\ x_{k,i}^{(G)} & \text{otherwise,} \end{cases} \quad (9)$$

where $x_{C_{k,i}}^{(G)}$ is the ‘‘donor’’, G is the current generation and i^* is a randomly selected integer within the interval $[1, n]$, computed once for all members of the population. The random number r is seeded for every chromosome parameter, while the DE control parameters $F \in [0, 1]$ and $C_r \in [0, 1]$ for the mutation and crossover operations, respectively, remain constant during the search process and affect the convergence behavior and robustness of the algorithm. Thereafter, at the selection stage, each trial vector $\mathbf{X}_k^{(G+1)}$ competes only against its counterpart (parent) in the

current population $\mathbf{X}_k^{(G)}$. The survivors of the N_p competitions being better fitted than the corresponding final candidates, move to the next generation. The DE selection scheme ensures the survival of the elitists, described as follows for a minimization problem:

$$\mathbf{X}_k^{(G+1)} = \begin{cases} \mathbf{X}_k^{(G+1)} & \text{if } f(\mathbf{X}_k^{(G+1)}) \leq f(\mathbf{X}_k^{(G)}), \\ \mathbf{X}_k^{(G)} & \text{otherwise.} \end{cases} \quad (10)$$

In most realistic applications, a classical DE algorithm requires a significant number of evaluations in order to succeed in delivering an adequate quality solution. Thus, in order to reduce the running time of the algorithm, two strategies have been explored in this work. More specifically, the DE algorithm was assisted by the introduction of surrogate models, which are used to substitute the computationally intensive exact evaluations of trial vectors with low-cost approximations, without compromising the robustness and the convergence of the DE algorithm [19], [20].

More precisely, the DE algorithm was combined with two Artificial Neural Networks (ANNs), a multi-layer perceptron (MLP) and a radial basis functions network (RBFN), which serve as surrogate models. In each generation, the two ANNs are re-trained to enhance their accuracy and predictive capability, while the most accurate of the two (based on their testing errors) is used in each generation for the pre-evaluations of the trial vectors. If a trial vector is pre-evaluated as better fitted than its parent, an exact evaluation is then performed; otherwise the trial vector is abandoned in favor of its parent. Parallel implementation was developed, based on MPI (Message Passing Interface) and the idea of ‘‘external-coupling’’ of the DE algorithm with the cost function evaluation software (i.e. the numerical solver of the GKT model in our case). A detailed description of the utilized parallel surrogate-assisted DE algorithm is presented in [19], [20].

B. Cost function formulation

As mentioned before, the optimization problem addressed herein consists of minimizing the deviation between the model calculations and the real-measured traffic data. Specifically, the model is fed with real measured boundary data [21] to produce the complete traffic state. For evaluation of the resulting model accuracy, three different cost functions have been tested, formulated in terms of discrete combinations of the speed, flow, and density values of real and simulated virtual detectors, within the simulated area. Specifically, a combined total mean square normalized errors of the model estimated and real measured speed and flow is used first, specifically

$$f(\mathbf{X}) = \frac{1}{C} \sum_{k=1}^K \sum_{i=1}^n \left[(1 - \mu) \left(1 - \frac{u_{i,k}}{u_{i,k}^d} \right)^2 + \mu \left(1 - \frac{q_{i,k}}{q_{i,k}^d} \right)^2 \right], \quad (11)$$

where μ is a weighting factor equal to 0.5. Alternatively, by substituting flow with density in equation above, the cost function is reformulated as

$$f(\mathbf{X}) = \frac{1}{C} \sum_{k=1}^K \sum_{i=1}^n \left[(1-\mu) \left(1 - \frac{u_{i,k}}{u_{i,k}^d} \right)^2 + \mu \left(1 - \frac{\rho_{i,k}}{\rho_{i,k}^d} \right)^2 \right]. \quad (12)$$

Moreover, by following the root mean square speed and density normalized errors the cost function is given as

$$f(\mathbf{X}) = \sqrt{\frac{1}{C} \sum_{k=1}^K \sum_{i=1}^n \left(\frac{u_{i,k}^d - u_{i,k}}{u_m^d} \right)^2} \sqrt{\frac{1}{C} \sum_{k=1}^K \sum_{i=1}^n \left(\frac{\rho_{i,k}^d - \rho_{i,k}}{\rho_m^d} \right)^2} \quad (13)$$

where, $u_{i,k}$, $\rho_{i,k}$, and $q_{i,k}$ represent, respectively, the predicted mean speed, density and flow, computed at detector location k (K is the number of detectors that are available for calibration) and time instant i (n is the simulation time horizon) and $C = nK$; $u_{i,k}^d$, $\rho_{i,k}^d$ and $q_{i,k}^d$ represent, respectively, the observed mean speed, density and flow computed at location k and time instant i , while u_m^d and ρ_m^d denote the corresponding maximum values of the observed mean speed and density.

The calibration procedure of the GKT model can be summarized as follows. At the beginning of the optimization procedure, an initial population is created by randomly initializing the parameter vectors \mathbf{X} (calibrated model parameters), within their predefined bounds. Each candidate solution (a vector \mathbf{X} of parameters for the GKT model) is used, along with the boundary input data, to set-up a numerical simulation for the traffic flow situation at hand and produces a space-time distribution of flow, speed and density. Subsequently, the cost function is computed for the corresponding candidate set of parameters, using one of (11), (12) and (13). The alteration, recombination and evaluation procedures of the DE algorithm are used to provide a new population of candidate vectors, with likely better cost function values. The evolution process is terminated when a pre-defined number of generations is reached.

IV. TEST NETWORK AND TRAFFIC DATA

The 9.45 km long 3-lane freeway stretch considered in this study is part of the M56 motorway in the United Kingdom, from Chester to Manchester. This 3-lane stretch includes one off-ramp and a two-lane on-ramp, which, before merging onto the motorway, splits into two separate lanes. In this work, a single lane with the mean values of the flow quantities of the 3-lane stretch is considered. Fig. 1 illustrates the layout of the simulated stretch, including the location of the on-ramps and off-ramp and the locations of the detectors.

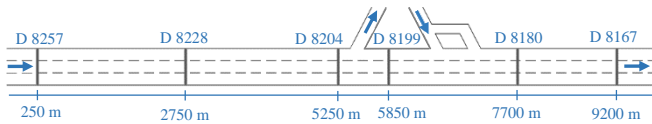


Figure 1. Layout of the considered 9.45 km freeway stretch in the U.K.

The real traffic data used in this work was provided by MIDAS database [21], including aggregate flow and speed measurements at the corresponding detector locations along the freeway, with a time resolution of 60 s. Measured data

corresponding to the stretch boundaries, including on/off ramps, were also available. The quantitative traffic data analysis showed that the chosen freeway stretch is subject to recurrent congestion that is induced by the high on-ramp flow in the morning rush hours. In particular, Fig. 2 (left) displays the space-time evolution of the real speed measurements for June 3rd, 2014, while Fig. 5 (left) for June 24th, 2014; it is observed that traffic congestion is formed upstream of the second on-ramp between 7–8 a.m. for both days; this congestion propagates upstream, creating an intensive low-speed area of several kilometers on the freeway mainstream.

V. CALIBRATION AND VALIDATION RESULTS

The numerically discretized GKT model is first calibrated to specify the optimal parameter values for the considered network, using the measured data for a specific day. Eventually, the GKT model is validated using data collected at the same freeway on a different day, to ensure that the model is able to reliably reproduce the traffic conditions of the examined site.

A. Calibration results

The calibration results were obtained using real traffic data from June 3rd. The model parameters with their corresponding feasible bounds, conform with those given in [15]–[18], are presented in Table I. The DE algorithm was employed with a population size equal to 50, whereas the maximum number of generations was set equal to 1100; the control parameters for the mutation and crossover operations were $F = 0.6$ and $C_r = 0.45$.

TABLE I. ADMISSIBLE RANGE OF THE PARAMETER VECTOR USED FOR THE GKT MODEL CALIBRATION

Model parameters	Units	Bounds
Desired free speed, u_{max} ,	km/h	[105, 135]
Maximum density, ρ_{max}	veh/km	[100, 200]
Critical density, ρ_{cr}	veh/km	[30, 60]
Desired time gap, T	s	[0.5, 2.5]
Anticipation factor, γ		[1, 2]
Relaxation time, τ	s	[10, 40]
Variance pre-factor for free traffic, A_0		[0.0025, 0.015]
Pre-factor, δA		[0.01, 0.03]
Transition width, $\delta \rho$	veh/km	[0.0035, 0.02]

The considered 9.45 km stretch was simulated for 3 morning peak hours (i.e. from 6 a.m. to 9 a.m.), whereas the space discretization was $\Delta x = 100$ m and the Courant-Friedrichs-Lewy (CFL) value was set equal to 0.5. The numerical scheme is stable under the usual CFL stability condition for explicit discretization schemes. The runs of the DE algorithm have been performed on a DELL PowerEdge R815 server with four 16-core, 2.5GHz processors (64 cores total). The clock computational time for 1100 generations was 146.5 min. Table II contains the minimum value of the three alternative cost functions (which were obtained in three respective optimization runs for the same calibration problem). Very good agreement with the measured data set and very similar optimal parameter vectors have been produced with all three cost functions; for brevity only the results for cost function (11) are presented next.

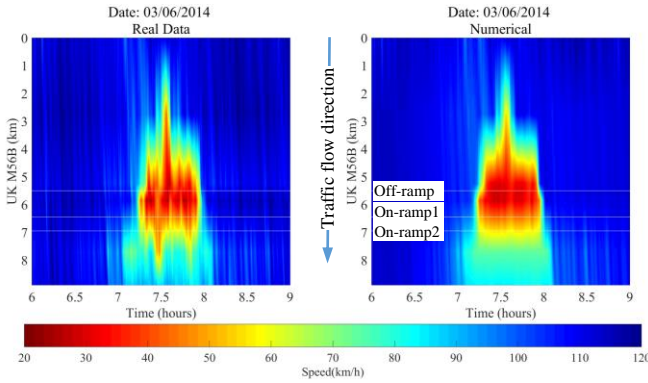


Figure 2. Phase space speed dynamics for real measured speed (left) and the model prediction (right) for the calibration date.

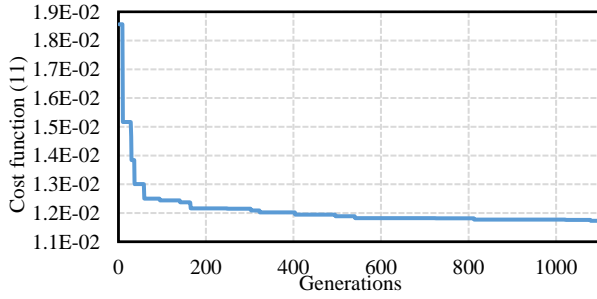


Figure 3. DE algorithm convergence history.

Fig. 2 displays the space time evolution of the speed reproduced by simulation compared to the observation for the calibration day. Fig. 3 contains the DE convergence history of the best value of the cost function in each generation, computed using (11). Figure 4 displays the speed dynamics for all detector locations, produced using the optimal parameter values of the calibration procedure with (11). The optimal parameters obtained for the three alternative cost functions are listed in Table III. It is clear that the real traffic conditions are well reproduced by the calibrated model, capturing with sufficient accuracy when and where the traffic flow becomes congested, for the correct duration and extent, as observed in the real traffic data.

TABLE II. COST FUNCTION VALUES FOR THE CALIBRATION PHASE

Cost Function	(11)	(12)	(13)
(%)	1.16	1.45	0.2

TABLE III. OPTIMAL MODEL PARAMETERS

Cost Function	u_{max} (km/h)	ρ_{max} (veh/km)	ρ_{cr} (veh/km)	T (s)	γ	τ (s)	A_0	δA	$\delta \rho$ (veh/km)
(11)	115	170	42	2	2	20	0.0025	0.015	10
(12)	120	150	40	2.3	2	24	0.0025	0.019	11
(13)	115	140	45	2.4	2	22	0.0025	0.027	12

B. Validation results

In order to assess the robustness of the produced calibrated parameters, the resulting GKT model was

validated using real traffic data in the same freeway stretch on a different day, which is June 24th, 2014, using the optimal parameters of the previous calibration procedure. The validation results presented in Fig. 5 (right) and Fig. 6, are seen to capture with sufficient accuracy the real traffic flow conditions in the particular freeway stretch, although not at the exact same level of accuracy as the calibrated ones. The cost function value for (11) for this validation procedure was 1.64 %.

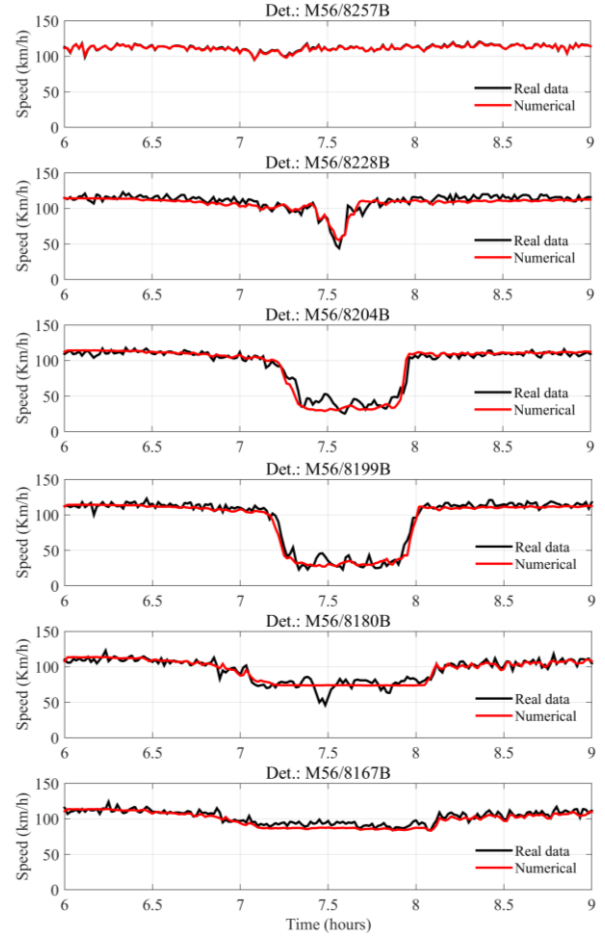


Figure 4. Time-series of the real speed measurements (black) and the model prediction of speed (red) at various detector locations for the calibration day.

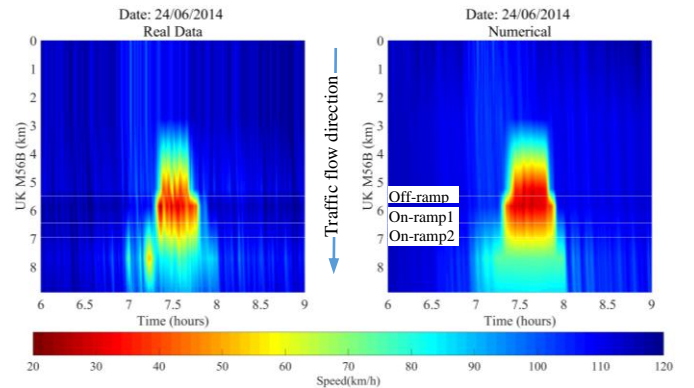


Figure 5. Phase space speed dynamics for real measured speed (left) and the model prediction (right) for the validation date.

VI. CONCLUSIONS

A recently developed parallel, metamodel-assisted DE algorithm was employed for the automated calibration of the parameters of a second-order GKT traffic flow model, using real traffic data. The macroscopic model has been numerically intergraded using a fifth-order in space finite-volume relaxation scheme. The calibration and validation results demonstrate a very good agreement with the corresponding measured data, showing that the GKT model is able to reproduce, with sufficient accuracy, the prevailing traffic conditions. The DE algorithm proved to be a useful and robust tool for the calibration of such macroscopic traffic flow models. It has the advantage that it can be used without the need of tuning its parameters for the problem at hand, while wide bounds can be used for the unknown vector without convergence problems. The well-known computational inefficiency of evolutionary algorithms was successfully addressed in our implementation with parallel processing and surrogate-model assistance.

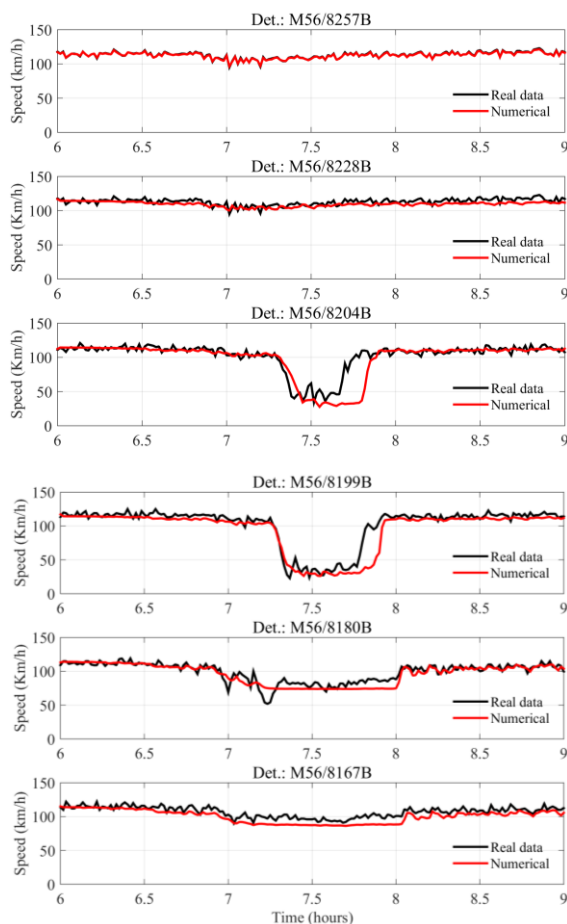


Figure 6. Time-series of the real speed measurements (black) and the model prediction of speed (red) at various detector locations for the validation day.

ACKNOWLEDGMENT

This research was supported by TRAFFIC MANAGEMENT for the 21st century (TRAMAN21) ERC Advanced Investigator Grand under the European Union's Seventh

Framework Program (FP/2007-20013). The authors are grateful to Highways England for providing access to the MIDAS data.

REFERENCES

- [1] S. P. Hoogendoorn and P. H. L. Bovy, "State-of-the-art of vehicular traffic flow modelling," *Proc. Inst. Mech. Eng. Part J. Syst. Control Eng.*, vol. 215, no. 4, pp. 283–303, Jun. 2001.
- [2] P. I. Richards, "Shock Waves on the Highway," *Oper. Res.*, vol. 4, no. 1, pp. 42–51, Feb. 1956.
- [3] H. J. Payne, "Models of Freeway Traffic and Control," *ResearchGate*, vol. 28, pp. 51–61, Jan. 1971.
- [4] M. Papageorgiou, "Some remarks on macroscopic traffic flow modelling," *Transp. Res. Part Policy Pract.*, vol. 32, no. 5, pp. 323–329, Sep. 1998.
- [5] M. Cremer and M. Papageorgiou, "Parameter identification for a traffic flow model," *Automatica*, vol. 17, no. 6, pp. 837–843, Nov. 1981.
- [6] M. Cremer and J. Ludwig, "A fast simulation model for traffic flow on the basis of boolean operations," *Math. Comput. Simul.*, vol. 28, no. 4, pp. 297–303, Aug. 1986.
- [7] M. Papageorgiou, J.-M. Blosseville, and H. Hadj-Salem, "Macroscopic modelling of traffic flow on the Boulevard Périphérique in Paris," *Transp. Res. Part B Methodol.*, vol. 23, no. 1, pp. 29–47, Feb. 1989.
- [8] K. K. Sanwal, K. Petty, J. Walrand, and Y. Fawaz, "An extended macroscopic model for traffic flow," *Transp. Res. Part B Methodol.*, vol. 30, no. 1, pp. 1–9, Feb. 1996.
- [9] A. Kotsialos, M. Papageorgiou, C. Diakaki, Y. Pavlis, and F. Middelham, "Traffic flow modeling of large-scale motorway networks using the macroscopic modeling tool METANET," *IEEE Trans. Intell. Transp. Syst.*, vol. 3, no. 4, pp. 282–292, Dec. 2002.
- [10] T. Monamy, H. Haj-Salem, and J.-P. Lebacque, "A Macroscopic Node Model Related to Capacity Drop," *Procedia - Soc. Behav. Sci.*, vol. 54, pp. 1388–1396, Oct. 2012.
- [11] D. Ngoduy, S. Hoogendoorn, and H. Van Zuylen, "Comparison of Numerical Schemes for Macroscopic Traffic Flow Models," *Transp. Res. Rec. J. Transp. Res. Board*, vol. 1876, pp. 52–61, Jan. 2004.
- [12] A. Spiliopoulou, M. Kontorinaki, M. Papageorgiou, and P. Kopelias, "Macroscopic traffic flow model validation at congested freeway off-ramp areas," *Transp. Res. Part C Emerg. Technol.*, vol. 41, pp. 18–29, Apr. 2014.
- [13] A. Spiliopoulou, I. Papamichail, M. Papageorgiou, I. Tyrinopoulos, and J. Chrysoulakis, "Macroscopic Traffic Flow Model Calibration Using Different Optimization Algorithms," *Transp. Res. Procedia*, vol. 6, pp. 144–157, 2015.
- [14] D. Ngoduy and M. J. Maher, "Calibration of second order traffic models using continuous cross entropy method," *Transp. Res. Part C Emerg. Technol.*, vol. 24, pp. 102–121, Oct. 2012.
- [15] A. I. Delis, I. K. Nikolos, and M. Papageorgiou, "High-resolution numerical relaxation approximations to second-order macroscopic traffic flow models," *Transp. Res. Part C Emerg. Technol.*, vol. 44, pp. 318–349, Jul. 2014.
- [16] D. Helbing, A. Hennecke, V. Shvetsov, and M. Treiber, "MASTER: macroscopic traffic simulation based on a gas-kinetic, non-local traffic model," *Transp. Res. Part B Methodol.*, vol. 35, no. 2, pp. 183–211, Feb. 2001.
- [17] M. Treiber, A. Hennecke, and D. Helbing, "Derivation, properties, and simulation of a gas-kinetic-based, nonlocal traffic model," *Phys. Rev. E*, vol. 59, no. 1, pp. 239–253, Jan. 1999.
- [18] M. Treiber and A. Kesting, *Traffic Flow Dynamics: Data, Models and Simulation*. Springer, 2013.
- [19] I. K. Nikolos, "On the use of multiple surrogates within a differential evolution procedure for high-lift airfoil design," *Int. J. Adv. Intell. Paradig.*, vol. 5, no. 4, pp. 319–341, Jan. 2013.
- [20] G. A. Strofylas and I. K. Nikolos, "Reverse Engineering of a Wind Turbine Blade Surface using Differential Evolution," in *Proceedings of the 4th International Conference on Soft Computing Technology in Civil, Structural and Environmental Engineering*, 2015.
- [21] Highways Agency. Motorway Incident Detection and Automatic Signalling (MIDAS) Design Standard, 1st ed., Bristol, UK, 2007.